THE JOURNAL OF PHYSICAL CHEMISTRY Letters

pubs.acs.org/JPCL

Improved Monodispersity of Plasmonic Nanoantennas via Centrifugal Processing

Timothy P. Tyler,[†] Anne-Isabelle Henry,[†] Richard P. Van Duyne,*[,†] and Mark C. Hersam*[,†,†]

[†]Department of Materials Science and Engineering and [†]Department of Chemistry, Northwestern University, Evanston, Illinois 60208-3108, United States

ABSTRACT Noble metal nanoparticle clusters underlie a variety of plasmonic devices and measurements including surface-enhanced Raman spectroscopy (SERS). Because of the strong dependence of plasmonic properties on nanoparticle cluster aggregation state, the elimination of non-SERS-active structures and the refinement of the nanoparticle cluster population are critical to realizing uniform and reproducible structures for plasmonic nanoantenna applications such as SERS-based sensors. In this Letter, we report a centrifugal sorting technique for gold core/silica shell nanoparticles that host SERS reporter molecules at the gold/silica interface. The relatively massive nanoparticle clusters are sorted by sedimentation coefficient via centrifugation in a high-viscosity density gradient medium, iodixanol, which yields solutions that contain a preponderance of one aggregation state and a diminished monomer population, as determined by transmission electron microscopy, extinction spectroscopy, and SERS. A quantitative analysis of the nanoparticle sedimentation coefficients is presented, thus allowing this approach to be predictably generalized to other nanoparticle systems.

SECTION Nanoparticles and Nanostructures

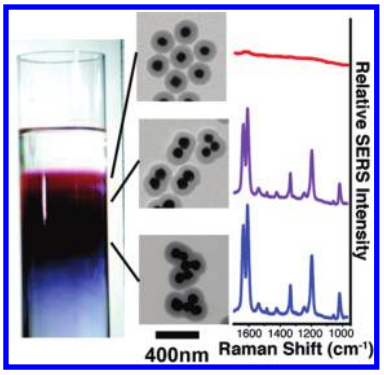

The intense electromagnetic field arising at the surface of metallic nanostructures from the excitation of the localized surface plasmon resonance (LSPR) allows for the enhancement of the Raman intensity of adsorbed molecules by a factor up to 4×10^8 or greater.[1] The structures supporting this plasmonic phenomenon, known as surface-enhanced Raman scattering (SERS), are diverse. The most sensitive examples, with an enhancement factor large enough to observe spectra at the single molecule level,[2−5] are aggregated metallic nanoparticles. Correlative structure−activity studies have indeed shown that the presence of a nanometer-sized junction[6,7] or crevice[1,8] creates the electromagnetic "hot-spot" (i.e., "nanoantenna") required to observe single-molecule SERS. Recent investigations of the hot-spots at the junction of silver cubes[9] and gold pyramidal shells[10] or at the interface between a gold nanostar and a gold surface[11] have highlighted how the control over the structure of this nanometer-scale region is crucial for achieving high enhancement factors. Whereas the early fundamental studies of single-molecule SERS have been performed on inhomogeneous samples, the integration of plasmonic nanoantennas into reliable technological applications, such as high sensitivity biological and chemical sensors, requires improved structural reproducibility.

Homogeneous nanostructure populations can be realized via precisely controlled fabrication or postsynthetic sorting techniques. Although much effort has been devoted to the controlled synthesis of nanoparticles, structural polydispersity remains an issue.[12−14] Consequently, postfabrication separation methods have become important for characterizing or refining populations of nanoparticles based on their size, shape, and aggregation state.[15] For example, electrophoretic methods,[16] most notably gel electrophoresis,[17] have been used to separate metal nanoparticles by both size and shape. Size-exclusion chromatography has also been demonstrated for separating gold nanoparticles by shape[18] and as a tool for characterizing synthesized nanoparticles.[19] In addition, sedimentation coefficient differences between nanoparticles of varying size and shape have been exploited for sorting by centrifugation[20] and sedimentation field-flow fractionation.[21] In particular, a recent study on polymer-coated nanoparticle clusters employed centrifugation and filtration to remove single-core nanoparticles and large aggregates, respectively, ultimately yielding samples of primarily multicore nanoparticle clusters with enhanced SERS signals.[22] Finally, density gradient centrifugation has proven to be particularly successful for obtaining refined populations of nanoparticles, leading to narrow diameter and shape distributions[23,24] or a specific aggregation state for nanoparticle clusters.[25]

For plasmonic applications, the removal of single nanoparticles from aggregates is particularly desirable given that only nanoparticle aggregates (i.e., two or more metallic nanoparticles) have thus far been shown to provide sufficient enhancement for single-molecule and single-particle SERS.[1,6]

Received Date: December 15, 2010
Accepted Date: January 10, 2011

DOI: 10.1021/jz101690f | *J. Phys. Chem. Lett.* 2011, *2*, 218–222

In particular, SERS nanoantennas consisting of aggregated spherical gold cores encapsulated in a protective silica shell with Raman reporter molecules adsorbed at the gold/silica interface have been shown to be ideal SERS substrates,[1,26] offering robustness and stability. The silica shell has the added benefit that it directly enables dispersion in aqueous solutions, thereby eliminating the need for additional chemical functionalization.

Here we report an effective method for sorting SERS-active silica-coated gold nanoparticle clusters by aggregation state in a high-viscosity density gradient. Whereas equilibrium isopycnic density gradient centrifugation techniques that are common for carbon-based nanomaterials[27−32] are incompatible with high-density structures such as nanoparticle clusters, sorting can, in principle, be accomplished by sedimentation coefficient in the transient centrifugal regime. However, in this study, the relatively large size of the gold cores (~100 nm in diameter) combined with the silica shell (~60 nm thick) makes sorting by transient motion challenging because these high-mass structures will sediment significantly faster than smaller nanoparticles. This issue is overcome by using the high-viscosity density gradient medium iodixanol, which slows the sedimentation of the gold/silica nanoparticle clusters to the point where structurally distinct fractions can be collected following centrifugation. Through transmission electron microscopy (TEM), extinction spectroscopy, and SERS characterization, the collected fractions are found to possess a preponderance of one aggregation state and a diminished monomer population, thus yielding ideal SERS nanoantennas that can be directly employed in a variety of plasmonic applications. In addition, the nanoparticle sedimentation coefficients are quantitatively analyzed, which will facilitate the application of this approach to other nanoparticle systems.

The as-synthesized gold core/silica shell nanoparticles (Cabot Security Materials) have the SERS reporter molecules (1,2-bis(4-pyridyl)ethylene (BPE)) adsorbed at the gold/silica interface and exist in a variety of aggregation states. A representative TEM image of the sample (HitachiHD2300 STEM operating at 200 kV in TE mode) is shown in Figure 1a, where the nanoparticles are found to exist as monomers or clusters that range from dimers to dodecamers with approximately spherical gold cores (96 ± 11 nm in diameter) encapsulated in a silica shell (63 ± 4 nm). Monomers represent more than half (59%) of the sample population, as shown in the population histogram (Figure 1b). The minority species include dimers (17%), trimers (11%), tetramers (7%), and pentamers (3%), with the remaining clusters possessing more than five cores. The bulk extinction spectrum of the nanoantennas suspended in water (Figure 1c) contains one peak centered at ~600 nm and a broader band centered at ~950 nm. Monomers of the size used here have a single plasmon resonance band and contribute strongly to the extinction at ~600 nm. Single-particle LSPR measurements have shown that dimers and trimers have two plasmon resonance bands.[1] The shorter wavelength band varies in position from ~650 to 850 nm depending on every structural detail but is particularly sensitive to the interparticle gap distance in the sub-2 nm range. Similarly, the width of the resonance depends sensitively on the structural details. The

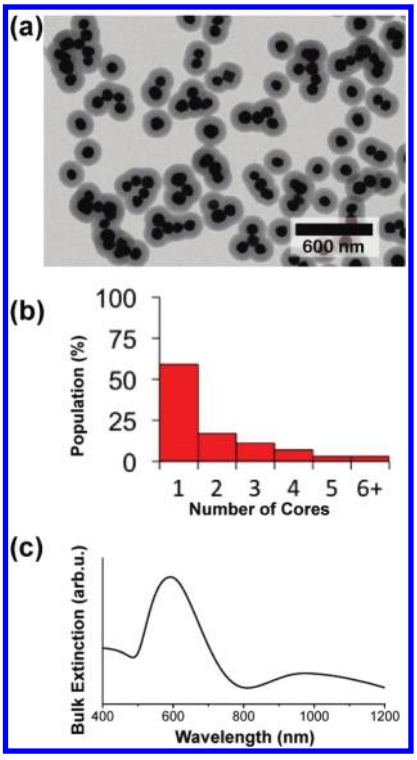

Figure 1. Characterization of the as-synthesized gold core/silica shell nanoparticle sample. (a) Representative TEM image showing the structure and variation in the number of gold cores within each silica shell. (b) Histogram of the population as a function of the number of cores. (c) Extinction spectrum of the as-synthesized sample dispersed in water.

longer wavelength band varies in position from ~800 to 1000 nm and is also structure sensitive. Consequently, dimers, trimers, and probably tetramers contribute to the extinction in the tail of the ensemble band at ~600 nm as well as to the blue leading edge of the ~950 nm band. Multicore clusters contribute the rest of the extinction for the ~950 nm band. Whereas the multicore clusters have demonstrated excellent SERS enhancement in previous correlated structure−SERS activity measurements performed on similar nanoparticles differing only by their reporter molecule,[1] no SERS signal is measured from monomers at low excitation power.

Centrifugal sorting was accomplished using a Beckman SW41Ti swinging bucket rotor. The centrifuge tubes were initially loaded with a linear density gradient of 30−60% weight per volume iodixanol (1.16 to 1.32 g cm^{-3}). Then, 200 μL of an aqueous suspension of the as-synthesized gold core/silica shell nanoparticles was carefully layered on top. Importantly, the silica coating allows the nanoparticles to be well-dispersed in water without the need for additional chemical functionalization or surfactants. After centrifuging at a relatively low speed (500g) for 10 min, a well-defined band and subsequent gradient of material is observed (Figure 2a).

Millimeter fractions were collected from the tube for TEM characterization using a piston gradient fractionator (Biocomp Instruments), and the resulting extinction spectra and aggregation state histograms (based on particle counting from the TEM images) for three of the fractions, labeled

DOI: 10.1021/jz101690f | J. Phys. Chem. Lett. 2011, 2, 218–222

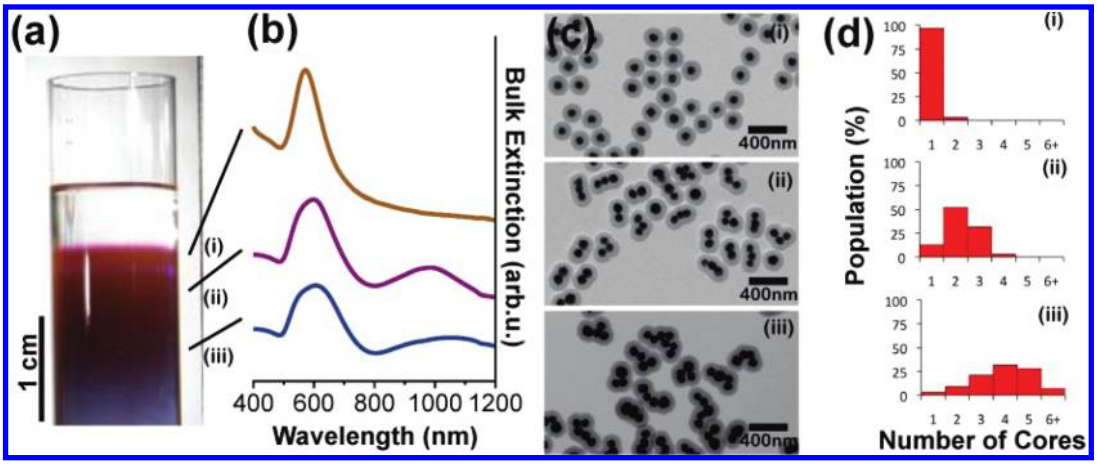

Figure 2. (a) Photograph of a centrifuge tube after centrifugation of the sample in a surfactant-free aqueous iodixanol linear density gradient. (b) Extinction spectra of three selected fractions, (i−iii), whose positions in the centrifugation tube are spatially indicated. (c) Corresponding TEM images of the selected fractions. (d) Corresponding population histograms of the selected fractions.

(i−iii), are shown in Figure 2. The extinction spectra were measured by UV−vis−NIR spectroscopy in solution for the collected fractions and are shown in Figure 2b. In the top band (i), only the surface plasmon band near 570 nm is present. For fractions at lower positions in the centrifuge tube, a new broad band in the near-IR known to correspond to multicore aggregates[33] is apparent, and the surface plasmon band is broadened and red-shifted. These spectra thus provide evidence that sorting by nanoparticle aggregation state has occurred with the top band likely enriched in monomers and subsequent bands possessing nanoparticle clusters. Analysis of the TEM images, as shown in Figure 2c, d, verifies this assignment by directly showing that the top band (i) contains almost exclusively monomers (97%), whereas subsequent fractions possess an increasing quantity and size of nanoparticle clusters. In particular, fraction (ii) consists of dimers (52%), trimers (32%), and monomers (13%), whereas fraction (iii) consists of tetramers (32%), pentamers (28%), trimers (21%), dimers (9%), and monomers (3%). Even though monomers are found outside the top band, at a sufficient tube depth, they are reduced to a negligible proportion of the population, thus implying fractions that consist almost exclusively of SERS-active nanoantennas.

Although this sorting method is highly effective at both removing monomers and targeting a narrow range of aggregation states, fractions other than the top band contain more than one nanoparticle aggregation state. To determine if this remaining polydispersity resulted from insufficient spatial separation of the bands in the centrifuge tube, imprecise fractionation, or both, the centrifugation time was increased to spread the sorted material over a larger length of the centrifuge tube. (See the Supporting Information.) Because this experiment provided minimal refinement compared with the original separation, the nanoclusters of differing aggregation states likely possess overlapping sedimentation coefficients. For example, the variability in gold core diameter and shell thickness yields a distribution of nanoparticle cluster mass and volume. The effect of this structural polydispersity on the sedimentation coefficient distribution is exacerbated at higher nanoparticle aggregation states, where multiple gold cores compound the variability in nanoparticle cluster mass and volume. Furthermore, nanoparticle clusters consisting of multiple gold cores can adopt a range of geometries (i.e., aspect ratios), which also influences the sedimentation coefficient.

To quantify the polydispersity in sedimentation coefficient as a function of nanoparticle aggregation state, we imaged a large number of nanoparticles (>600) from the as-synthesized sample. The core diameters and aspect ratios were then individually extracted from the TEM data. The sedimentation coefficient can then be calculated using the following equation

$$s = \frac{m(1-\rho_s/\rho_p)}{f} \quad (1)$$

where m is the total particle mass, ρ_s and ρ_p are the densities of the solvent and particle, respectively, and f is the frictional coefficient, which depends on the shape of the nanoparticle and the viscosity of the solvent. To account for the observed variation in shape (Figure S2 of the Supporting Information), the nanoparticle clusters were modeled as prolate ellipsoids using the total volume of gold obtained from the core diameters, the average silica shell thickness, and the individually measured aspect ratios. The frictional coefficient was then calculated using the Perrin equation for frictional ratios of ellipsoids of revolution,[34] which modifies the frictional coefficient of a sphere with a geometrical correction factor P as follows

$$f_{\text{ellipsoid}} = P(3\pi\eta d),$$
$$\text{where } P = (1-q^2)^{1/2}/[q^{2/3}(\ln(\{1+(1-q^2)^{1/2}\}/q))] \quad (2)$$

Here η is the viscosity of the solvent, d is the effective diameter of the equivalent sphere, and q is the aspect ratio of the prolate ellipsoid, where $q < 1$.

Using this ellipsoidal model and the structural parameters extracted from TEM, we calculated the distribution of

DOI: 10.1021/jz101690f | J. Phys. Chem. Lett. 2011, 2, 218–222

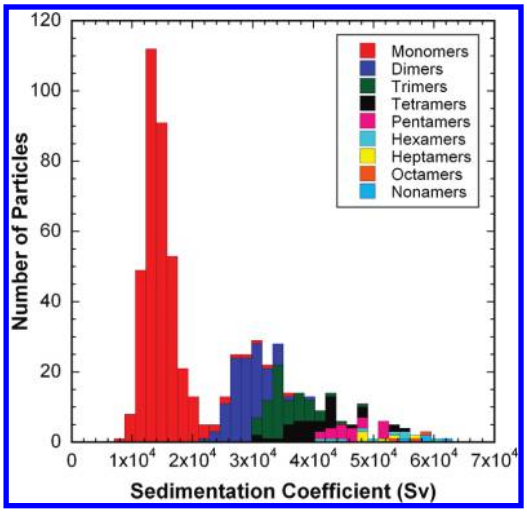

Figure 3. Histogram of sedimentation coefficients for varying aggregation states, calculated by applying a Perrin ellipsoid model to individually measured nanoclusters. This model predicts high purity separation of monomers, followed by overlapping domains of dimers, trimers, tetramers, and higher order clusters, in agreement with the experimental data.

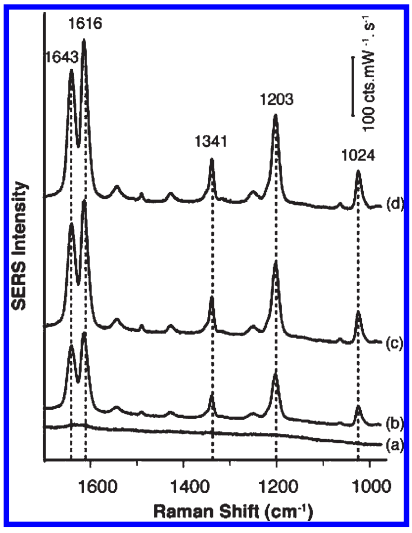

Figure 4. Measured SERS spectra of 1,2-bis(4-pyridyl)ethylene (BPE), from (a) fraction (i), (b) the initial solution, (c) fraction (ii) enriched in dimers, and (d) fraction (iii) enriched in tetramers when illuminated at a 632.8 nm excitation wavelength and power of 6.0 mW.

sedimentation coefficients for the as-synthesized sample at a fixed point (40% w/v iodixanol, 1.21 g cm^{-3}) in the density gradient[35] (Figure 3). This model reveals the presence of a monomer band at low sedimentation coefficients, followed by a gap in sedimentation coefficient, and finally overlapping aggregation states at higher sedimentation coefficients. Consequently, transient centrifugal sorting is expected to yield highly enriched monomers at the top of the centrifuge tube and then increasing but overlapping levels of nanoparticle aggregation for subsequent fractions, in agreement with the experimental results. This model thus holds promise for evaluating the feasibility of and refining the experimental conditions for sorting other nanoparticle clusters via transient density gradient centrifugation techniques, assuming that the initial nanoparticle structural parameters and polydispersity have been determined. Conversely, the results of transient density gradient centrifugation experiments can provide quantitative insight into the structural polydispersity of nanoparticle samples.

To show the utility of the sorted nanoparticle clusters, ensemble averaged SERS measurements were performed on the initial solution and the selected fractions (i−iii). The nanoparticle concentrations were balanced between the samples using the visible surface plasmon band in the extinction spectra. The SERS spectra of 1,2-bis(4-pyridyl)ethylene (BPE) were collected using excitation at a wavelength of 632.8 nm and power of 6 mW (HeNe laser 17 mW from Research Electro-optics). The spectra were acquired for 15 s with three accumulations. The fraction enriched in monomers (i) exhibited no peaks; that is, no SERS signal was observed (spectrum (a), Figure 4), which is in agreement with previously published results on similar SERS nanoantennas.[1] The initial solution (spectrum (b), Figure 4) exhibited the characteristic peaks of BPE including 1616, 1643, 1203, 1341, and 1024 cm^{-1} in decreasing intensity. The same peaks were observed with the same intensity ratio on the measured SERS spectra from the fractions enriched in dimers and trimers (ii) (spectrum (c), Figure 4) and tetramers (iii) (spectrum (d), Figure 4). The intensities of the peaks from the sorted fractions, where the amount of monomers has been substantially reduced, are higher than those for the initial solution. This increase in SERS signal is further evidence that centrifugal sorting has yielded samples enriched in SERS-active nanoantennas.

In summary, we have demonstrated a facile, surfactant-free method for sorting high-mass silica-coated gold nanoparticle clusters by aggregation state via transient density gradient centrifugation. The improved monodispersity of the nanoparticle clusters is quantified by TEM, extinction spectroscopy, and SERS. Furthermore, a quantitative model is presented that accurately mirrors the observed sorting results and provides guidance to future efforts to separate other nanoparticles in the transient sedimentation regime. By removing non-SERS-active monomers and narrowing the nanoparticle aggregation state distribution, density gradient centrifugation serves as an effective postsynthetic processing technique for realizing uniform and reproducible structures for plasmonic nanoantenna applications such as SERS-based sensors.

SUPPORTING INFORMATION AVAILABLE

Additional experimental parameters, characterization methods, and TEM images. This material is available free of charge via the Internet at http://pubs.acs.org.

AUTHOR INFORMATION

Corresponding Author:

*To whom correspondence should be addressed. E-mail: (R.P.V.D.) vanduyne@northwestern.edu; (M.C.H.) m-hersam@northwestern.edu.

ACKNOWLEDGMENT This work was supported by the National Science Foundation (CHE-0911145, DMR-0520513, and DMR-1006391); the ANSER center, an Energy Frontier Research Center

DOI: 10.1021/jz101690f | J. Phys. Chem. Lett. 2011, 2, 218–222

funded by the U.S. Department of Energy (DE-SC0001059); and AFSOR/DARPA Project BAA07-61 (FA9550-08-1-0221). We thank Dr. R. Griff Freeman and Dr. Michael J. Natan from Cabot Security Materials for providing the SERS nanoantenna samples. STEM experiments were performed in the EPIC Facility of the NUANCE Center at Northwestern University. NUANCE is supported by the NSF-NSEC, NSF-MRSEC, Keck Foundation, State of Illinois, and Northwestern University.

REFERENCES

(1) Wustholz, K. L.; Henry, A.-I.; McMahon, J. M.; Freeman, R. G.; Valley, N.; Piotti, M. E.; Natan, M. J.; Schatz, G. C.; Van Duyne, R. P. Structure-Activity Relationships in Gold Nanoparticle Dimers and Trimers for Surface-Enhanced Raman Spectroscopy. *J. Am. Chem. Soc.* **2010,** *132*, 10903–10910.

(2) Kneipp, K.; Wang, Y.; Kneipp, H.; Perelman, L. T.; Itzkan, I.; Dasari, R. R.; Feld, M. S. Single Molecule Detection Using Surface-Enhanced Raman Scattering (SERS). *Phys. Rev. Lett.* **1997,** *78*, 1667–1670.

(3) Nie, S. M.; Emory, S. R. Probing Single Molecules and Single Nanoparticles by Surface-Enhanced Raman Scattering. *Science* **1997,** *275*, 1102–1106.

(4) LeRu, E. C.; Meyer, M.; Etchegoin, P. G. Proof of Single-Molecule Sensitivity in Surface Enhanced Raman Scattering (SERS) by Means of a Two-Analyte Technique. *J. Phys. Chem. B* **2006,** *110*, 1944–1948.

(5) Dieringer, J. A.; Lettan, R. B., II; Scheidt, K. A.; Van Duyne, R. P. A Frequency Domain Existence Proof of Single-Molecule Surface-Enhanced Raman Spectroscopy. *J. Am. Chem. Soc.* **2007,** *129*, 16249–16256.

(6) Michaels, A. M.; Jiang, J.; Brus, L. Ag Nanocrystal Junctions as the Site for Surface-Enhanced Raman Scattering of Single Rhodamine 6G Molecules. *J. Phys. Chem. B* **2000,** *104*, 11965–11971.

(7) Camden, J. P.; Dieringer, J. A.; Wang, Y.; Masiello, D. J.; Marks, L. D.; Schatz, G. C.; Van Duyne, R. P. Probing the Structure of Single-Molecule Surface-Enhanced Raman Scattering Hot Spots. *J. Am. Chem. Soc.* **2008,** *130*, 12616–12617.

(8) Moskovits, M.; Jeong, D. H. Engineering Nanostructures for Giant Optical Fields. *Chem. Phys. Lett.* **2004,** *397*, 91–95.

(9) Rycenga, M.; Camargo, P. H. C.; Weiyang, L.; Moran, C. H.; Xia, Y. Understanding the SERS Effects of Single Nanoparticles and Their Dimers, One at a Time. *J. Phys. Chem. Lett.* **2010,** *1*, 696–703.

(10) Stoerzinger, K. A.; Hasan, W.; Lin, J. Y.; Robles, A.; Odom, T. W. Screening Nanopyramid Assemblies to Optimize Surface Enhanced Raman Scattering. *J. Phys. Chem. Lett.* **2010,** *1*, 1046–1050.

(11) Alvarez-Puebla, R.; Liz-Marzán, L. M.; García de Abajo, F. J. Light Concentration at the Nanometer Scale. *J. Phys. Chem. Lett.* **2010,** *1*, 2428–2434.

(12) Jana, N. R.; Gearheart, L.; Murphy, C. J. Wet Chemical Synthesis of High Aspect Ratio Cylindrical Gold Nanorods. *J. Phys. Chem. B* **2001,** *105*, 4065–4067.

(13) Xia, Y.; Xiong, Y.; Lim, B.; Skrabalak, S. E. Shape-Controlled Synthesis of Metal Nanocrystals: Simple Chemistry Meets Complex Physics? *Angew. Chem., Int. Ed.* **2009,** *48*, 60–103.

(14) Wiley, B.; Sun, Y.; Mayers, B.; Xia, Y. Shape-Controlled Synthesis of Metal Nanostructures: The Case of Silver. *Chem.—Eur. J.* **2005,** *11*, 454–463.

(15) Liu, F.-K. Analysis and Applications of Nanoparticles in the Separation Sciences: A Case of Gold Nanoparticles. *J. Chromatogr. A* **2009,** *1216*, 9034–9047.

(16) Hanauer, M.; Pierrat, S.; Zins, I.; Lotz, A.; Sönnichsen, C. Separation of Nanoparticles by Gel Electrophoresis According to Size and Shape. *Nano Lett.* **2007,** *7*, 2881–2885.

(17) Surugau, N.; Urban, P. L. Electrophoretic Methods for Separation of Nanoparticles. *J. Sep. Sci.* **2009,** *32*, 1889–1906.

(18) Wei, G. T.; Liu, F. K.; Wang, C. R. C. Shape Separation of Nanometer Gold Particles by Size-Exclusion Chromatography. *Anal. Chem.* **1999,** *71*, 2085–2091.

(19) Liu, F.-K. SEC Characterization of Au Nanoparticles Prepared through Seed-Assisted Synthesis. *Chromatographia* **2007,** *66*, 791–796.

(20) Sharma, V.; Park, K.; Srinivasarao, M. Shape Separation of Gold Nanorods Using Centrifugation. *Proc. Natl. Acad. Sci. U.S.A.* **2009,** *106*, 4981–4985.

(21) Contado, C.; Argazzi, R. Size Sorting of Citrate Reduced Gold Nanoparticles by Sedimentation Field-Flow Fractionation. *J. Chromatogr. A* **2009,** *1216*, 9088–9098.

(22) Braun, G. B.; Lee, S. J.; Laurence, T.; Fera, N.; Fabris, L.; Bazan, G. C.; Moskovits, M.; Reich, N. O. Generalized Approach to SERS-Active Nanomaterials via Controlled Nanoparticle Linking, Polymer Encapsulation, and Small-Molecule Infusion. *J. Phys. Chem. C* **2009,** *113*, 13622–13629.

(23) Sun, X.; Tabakman, S. M.; Seo, W.-S.; Zhang, L.; Zhang, G.; Sherlock, S.; Bai, L.; Dai, H. Separation of Nanoparticles in a Density Gradient: FeCo@C and Gold Nanocrystals. *Angew. Chem., Int. Ed.* **2009,** *48*, 939–942.

(24) Bai, Lu.; Ma, X.; Liu, J.; Sun, X.; Zhao, D.; Evans, D. E. Rapid Separation and Purification of Nanoparticles in Organic Density Gradients. *J. Am. Chem. Soc.* **2010,** *132*, 2333–2337.

(25) Chen, G.; Wang, Y.; Tan, L. H.; Yang, M.; Tan, L. S.; Chen, Y.; Chen, H. High-Purity Separation of Gold Nanoparticle Dimers and Trimers. *J. Am. Chem. Soc.* **2009,** *131*, 4218–4219.

(26) Doering, W. E.; Piotti, M. E.; Natan, M. J.; Freeman, R. G. SERS as a Foundation for Nanoscale, Optically Detected Biological Labels. *Adv. Mater.* **2007,** *19*, 3100–3108.

(27) Arnold, M. S.; Green, A. A.; Hulvat, J. F.; Stupp, S. I.; Hersam, M. C. Sorting Carbon Nanotubes by Electronic Structure Using Density Differentiation. *Nat. Nanotechnol.* **2006,** *1*, 60–65.

(28) Hersam, M. C. Progress Towards Monodisperse Single-Walled Carbon Nanotubes. *Nat. Nanotechnol.* **2008,** *3*, 387–394.

(29) Green, A. A.; Hersam, M. C. Solution Phase Production of Graphene with Controlled Thickness via Density Differentiation. *Nano Lett.* **2009,** *9*, 4031–4036.

(30) Green, A. A.; Hersam, M. C. Emerging Methods for Producing Monodisperse Graphene Solutions. *J. Phys. Chem. Lett.* **2010,** *1*, 544–549.

(31) Green, A. A.; Hersam, M. C. Processing and Properties of Highly Enriched Double-Wall Carbon Nanotubes. *Nat. Nanotechnol.* **2009,** *4*, 64–70.

(32) Liu, L.; Hersam, M. C. Recent Developments in Carbon Nanotube Sorting and Selective Growth. *MRS Bull.* **2010,** *35*, 315–321.

(33) Norman, T. J., Jr.; Grant, C. D.; Magana, D.; Zhang, J. Z. Near Infrared Optical Absorption of Gold Nanoparticle Aggregates. *J. Phys. Chem. B* **2002,** *106*, 7005–7012.

(34) Perrin, F. Mouvement Brownien d'un Ellipsoide (II). Rotation Libre et Dépolarisation des Fluorescences. Translation et Diffusion de Molécules Ellipsoidales. *J. Phys. Radium* **1936,** *7*, 1–11.

(35) Eivindvik, K.; Sjøgren, C. E. Physicochemical Properties of Iodixanol. *Acta Radiol. Suppl.* **1995,** *399*, 32–38.

DOI: 10.1021/jz101690f | *J. Phys. Chem. Lett.* **2011,** *2*, 218–222